European Polymer Journal 154 (2021) 110536

Contents lists available at ScienceDirect

European Polymer Journal

journal homepage: www.elsevier.com/locate/europolj

Photopolymerizable precursors for degradable biomaterials based on acetal moieties

Barbara Dellago [a,b,c], Alexander Ricke [b,c], Theresa Geyer [a,b,c], Robert Liska [b,c], Stefan Baudis [a,b,c,*]

[a] Christian Doppler Laboratory for Advanced Polymers for Biomaterials and 3D Printing, Getreidemarkt 9, 1060 Vienna, Austria
[b] Institute of Applied Synthetic Chemistry, TU Wien, Getreidemarkt 9/163 MC, 1060 Vienna, Austria
[c] Austrian Cluster for Tissue Regeneration, 1200 Vienna, Austria

ARTICLE INFO

Keywords:
Photoprecursors
Photopolymers
Cleavable functionality
Biocompatibility

ABSTRACT

In tissue engineering (TE), artificial biomaterials have emerged over the past decade as an alternative to autotransplants. The main characteristics of these materials include good biocompatibility as well as biodegradability. Up to now, most materials used in TE are based on polyesters, which are limited in their scope of application, especially as scaffolds, due to their undesirably slow degradation behavior under acidic conditions present, *e.g.* during the process of hydroxyapatite resorption during bone regeneration. Furthermore, the formation of acidic degradation products can lead to tissue inflammation or even necrosis. Therefore, alternatives to ester functionalities, which show enhanced degradability under acidic conditions, are of interest. Herein, we present the synthesis of linear and cyclic acetal-based monomers for photopolymerizable materials. The reactivity and mechanical properties of polymer networks derived from these monomers were investigated. Moreover, their degradation behavior compared to ester-based polymer networks was explored. Degradation studies of the model compounds showed that the synthesized acetals degrade 80 to 200 times faster than their ester counterparts. A subsequent *in vitro* degradation study of polymer networks based on these compounds confirmed the potential of acetals moieties in polymeric biomaterials for bone regeneration.

1. Introduction

Over the past decades, the demand for bone replacement materials is on the rise. Age–related problems in the rapidly aging society of developed nations, such as musculoskeletal or cardiovascular diseases, contribute to this trend. Today, arthroplastic surgical procedures, such as hip joint replacements, are everyday orthopedic practice. Furthermore, the recent developments in minimally invasive surgeries, especially in the orthopedic fields of spine surgery [1], increased the need for bone grafts. Although bone tissue has the ability to regenerate, the coalescence process often fails in the case of major bone fractures or significant pathological bone losses [2]. In these cases, massive scaffolds are needed to ensure a successful regeneration process. This wide range of applications make bone structures the second most transplanted tissue after blood [3,4].

The "gold standard" for conventional treatments of bone defects is autotransplantation of tissue [5]. Within this procedure, tissue is taken from and transplanted to the same patient [6]. This means autografts are natural bone substitutes and thus, from a biological point of view, the best material available because it bears a low immunogenic potency combined with a strong ability for incorporation into the host site [7].

The main drawback of this technique is that patients who need tissue replacements are often affected by multiple conditions and are thus too unstable for exhausting operations like autotransplantations. The additional surgery causes donor pain and has an increased potential for complications like major vessel and visceral injuries, hematomas, or fractures [7–9]. Indeed, the reported morbidity rate for the donor site is approximately 20% in all cases [10,11]. Furthermore, the amount of graft material is restricted, and sufficient amounts of autografts are often not available for massive grafts [12,13].

An answer to all these restrictions could be synthetic bone substitutes. Within the scientific field of tissue engineering (TE), the development of artificial tissue scaffolds can offer an effective treatment strategy for skeletal conditions without a need for risky autotransplants.

In an ideal case, the bone scaffolds should completely degrade within an adequate time. If the degradation rate is too fast, the scaffold cannot

* Corresponding author at: Getreidemarkt 9/163 MC, 1060 Vienna, Austria.
E-mail address: stefan.baudis@tuwien.ac.at (S. Baudis).

https://doi.org/10.1016/j.eurpolymj.2021.110536
Received 5 November 2020; Received in revised form 20 May 2021; Accepted 23 May 2021
Available online 26 May 2021

provide sufficient support for the construction of new bone tissue. Yet, a too slow degradation rate can suppress the formation of bone tissue [14].

The process of bone-regeneration consists of both bone resorption and bone formation. In these processes two different types of cells take part. Osteoclasts are involved in the bone resorption [15–17] and osteoblasts are involved in the regeneration of the new bone matrix [18]. For the process of osteoclast-driven bone resorption, a pH below 4.5 is essential [19,20]. Only under these acidic conditions, the mineral hydroxyapatite, the main component of bone structures, is soluble. Indeed, to resorb the bone matrix, osteoclasts form an extracellular compartment between their cell wall and the bone surface in which pH values of 3 or even lower can be measured [16,21,22].

Natural polymers used in bone regeneration are collagen, gelatin and fibrin [23]. Composites of collagen and calcium phosphates are already used in orthopedic surgeries as fillers to repair minor bone defects [24]. Gelatin can be found in coatings for drugs or as a component for degradable hydrogels applied in tissue engineering [25–27]. The advantage of these biomaterials is the rapid *in vivo* degradation catalyzed by enzymes [28,29].

Most of the reported and applied artificial materials in TE, which are worth considering for skeletal bone scaffolds are based on an ester polymer backbone, *e.g.* poly(hydroxy acids) like poly(ε–caprolactone) (PCL), poly(glycolic acid) (PGA), and poly(lactic acid) (PLA), poly(anhydrides) like poly(carboxyphenoxypropane) (PCCP), and poly(carbonates) like poly(DTR carbonate) (DTR = desaminotyrosyl tyrosine alkyl ester) [30–32].

Under the acidic conditions created by the osteoblasts to resorb the bone structure, materials containing esters as cleavable moieties degrade too slow. Furthermore, ester degradation releases acidic products, contributing to an increase in inflammation and potential tissue necrosis [33]. For this reason, alternatives to esters must be developed to push the limitations of bone scaffolds for skeletal conditions. Our approach is to incorporate acetals as degradable functional groups into the polymer materials.

In contrast to esters, acetals seem to be suitable because they cleave rapidly under acidic conditions. Furthermore, acetals form alcohol and aldehyde moieties as degradation products, yielding significantly milder pH when compared to an ester degradation. However, aldehydes are very reactive functional groups and can couple, *e.g.* with free amino groups of proteins. This might lead to the denaturation of proteins and is one of the reasons aldehydes are toxic compounds. The toxicity of aliphatic aldehydes is decreasing with an increasing chain length and saturated aldehydes are more biocompatible in comparison to unsaturated aldehydes [34].

The acetal hydrolysis is not an autocatalytic reaction, thus a more homogeneous degradation of acetal–based biomaterials is expected when compared to biomaterials with incorporated ester groups. The structural variation of acetal moieties from linear to cyclic allows to adjust and fine–tune the degradation speed of scaffolds to a desired rate [35]. Nowadays, additive manufacturing technologies such as 3D printing play a key role in bone-regeneration strategies using tissue engineering. They allow to create scaffolds with a shape explicitly adjusted to the anatomical details obtained from the patient [36]. The developed materials containing acetal moieties as degradable groups should thus be applicable as photopolymerizable precursors in 3D printing. Additionally, these materials can also be cured under mild, physiological conditions.

In this work, we describe the synthesis of linear as well as cyclic acetals as photopolymerizable precursors for biomaterials. The network formation of the photopolymers is investigated with the help of RT–FTNIR–photorheology and the mechanical properties are further studied by dynamic mechanical thermal analysis. The rate of degradation for linear and cyclic acetals is determined *via* ^{1}H NMR experiments. Furthermore, the swelling and degradation rate of the photopolymer networks were determined at a physiological pH of 2.2. This pH value can occur in the extracellular compartment of the osteoclasts during the process of bone regeneration [22].

Other approaches making use of acetal moieties as degradable structures in tissue engineering were published by Betz *et al.* [37–40]. These works focused on the synthesis of hydrogels containing six membered cyclic acetals. The applicability of the materials to repair bone defects were tested thoroughly *e.g.* in cell seeding experiments and cytotoxicity studies. In contrast to our work the developed materials are rather suitable as scaffolds for the replacement of soft tissue. Furthermore, the materials were not photopolymerizable and not applicable for additive manufacturing. In another notable work, done by Alameda *et al.* [41], hydrolytically degradable thermosets containing a broad range of five membered cyclic acetals were synthesized. The main focus of this work was on the recyclability of the resulting polymers, thus the degradation studies were conducted at a pH 0.2, 7.4 and 13.5 which are rather harsh conditions and not applicable in TE. In a recently published work by Sycks *et al.* [42,43], spiroacetals have been utilized to synthesize tough semicrystalline thiol-ene photopolymers, which are applicable for additive manufacturing. No degradation studies were conducted as the material was not designed for the application in tissue engineering. In a publication by Lingier *et al.* [44] a large–scale synthesis of rigid spiroacetals was presented. The synthesized acetal containing thermoplastics had rather high glass transition temperature for up to 85 °C but within the acid-mediated degradation study no degradation was monitored, what makes the material less interesting for TE applications.

2. Experimental section

2.1. Materials and general methods

Valeraldehyde (TCI), 2-hydroxyethyl methacrylate (HEMA, Sigma-Aldrich), glycidyl methacrylate (TCI), terephthalaldehyde (Sigma-Aldrich), 4–formylbenzoic acid (BLD Pharmatech ltd.), glycerol (Fluka), lithium aluminum hydride ($LiAlH_4$, Fluka), 4–methylbenzene–1–sulfonic acid (*p*TsOH, TCI), ammonium chloride (NH_4Cl, Carl Roth), 1,4–benzenedimethanol (TCI), methacryloyl chloride (Sigma–Aldrich), 4–methoxyphenol (MEHQ, Sigma–Aldrich) and phenothiazine (Sigma–Aldrich) were purchased from respective companies and used as received unless otherwise noted. The photoinitiator bis(4-methoxybenzoyl)diethylgermanium (Ivocerin®) and the monomer 1,10–decanediol dimethacrylate (**D3MA**) were kindly provided by Ivoclar Vivadent AG and used as received. Commercial grade tetrahydrofuran (THF, Donau Chemie) was dried using a PureSolvsystem (Inert, Amesbury, MA). Petroleum ether (PE, Donau Chemie), ethyl acetate (EE, Donau Chemie), acetonitrile (ACN, 99.9% HPLC, VWR) and chloroform ($CHCl_3$, Acros Organics) were used without further purification. All monomers were used without removal of inhibitor.

NMR Spectra. NMR spectra were recorded on a Bruker Avance at 400 MHz for ^{1}H (100 MHz for ^{13}C) at room temperature. The samples were dissolved in $CDCl_3$ or DMSO–d_6 and referenced to the solvent residual peak. Chemical shifts are given in ppm, multiplicities are termed s (singlet), d (doublet), t (triplet), q (quartet), and m (multiplet), and coupling constants (*J* values) are given in hertz. The data were processed with the software TopSpin 3.5 pl 7 from Bruker.

Refraction Index. The refraction index n_D^{20} was measured with a Carl Zeiss Abbe refractometer with a Na lamp at 20 °C.

pH–Evaluation. pH-Values were determined with a pH 340i pocket meter and a SI Analytics® pH electrode BlueLine pH 14.

HPLC Measurements. HPLC measurements were performed with a modular HP Agilent 1100 device, equipped with an HP photodiode array detector and a quaternary gradient pump. An OUT LipoMare C18 (105 Å; 5 μm, 150 × 4 mm) reversed-phase column was used at a flow rate of 0.7 mL min^{-1} with an eluent system of H_2O:ACN = 42:58 or H_2O:ACN = 70:30 for separation. The device was equipped with an autosampler, and

the software ChemStation for LC 3D systems from Ailent Technologies (vB03.02-SR2).

Melting points. Melting points were measured on an OptiMelt automated melting point system from SRS Stanford Research System. The heating rate was set to 2 °C min^{-1}.

HR–MS Measurements. The analysis was carried out in acetonitrile solutions (concentration: 10 μM) by using an HTC PAL system autosampler (CTC Analytics AG, Zwingen, Switzerland), an Agilent 1100/1200 HPLC with binary pumps, degasser and column thermostat (Agilent Technologies, Waldbronn, Germany) and Agilent 6230 AJS ESI–TOF mass spectrometer (Agilent Technologies, Palo Alto, United States). Data evaluation was performed using Agilent MassHunter Qualitative Analysis B.07.00. Identification was based on peaks obtained from extracted ion chromatograms (extraction width ± 20 ppm).

2.2. Monomer synthesis and characterization

2.2.1. Synthesis of 1,1′-[pentanebis(oxy-2,1-ethanediyl)]-2-methyl-2-propenoic acid ester (*AlLA*)

For the synthesis of **AlLA**, valeraldehyde (3.02 g, 34.8 mmol), HEMA (18.14 g, 139.9 mmol), *p*-TsOH (66.3 mg, 0.3 mmol), MEHQ (1000 ppm), and phenothiazine (300 ppm) were placed in a 500 mL three-necked flask (purged with argon) and dissolved in 200 mL chloroform. The reaction mixture stirred at reflux for 3 days with an inverse Dean–Stark apparatus. The solution was extracted with sat. $NaHCO_3$ solution (4 × 40 mL), washed with deionized water (10 × 20 mL) and brine (2 × 30 mL). The combined organic phases were dried with Na_2SO_4 and filtered. The organic solvent was evaporated under reduced pressure. The crude product was purified *via* flash column chromatography on silica gel (petrol ether/triethylamine 5 vol%) and isolated with a yield of 8.51 g (74% calculated yield) as a light yellow liquid. n_D^{20} = 1.456. HR–MS: calc. EM + Na: 351.1783 g/mol; found: 351.1793 g/mol. ^{1}H NMR (400 MHz, DMSO–d_6) δ (ppm): 6.02 (d, *J* = 1.6 Hz, 2H, C=CH–H), 5.68 (dh, *J* = 3.2, 1.6 Hz, 2H, C=CH–H), 4.61 – 4.52 (m, 1H, CH–$(O–)_2$), 4.21 (dd, *J* = 5.5, 4.0 Hz, 4H, OCH_2CH_2O), 3.74 (ddd, *J* = 9.3, 6.5, 4.0 Hz, 2H, OCH_2CH_2O), 3.69 – 3.62 (m, 2H, OCH_2CH_2O), 1.88 (dd, *J* = 3.3, 2.0 Hz, 6H, C–CH_3), 1.57 – 1.48 (m, 2H, $(–O)_2$–CH–CH_2–), 1.26 (dt, *J* = 8.3, 3.9 Hz, 4H, –CH–CH_2–CH_2–), 0.88 – 0.80 (m, 3H, –CH–CH_2–CH_2–CH_3). ^{13}C NMR (100 MHz, DMSO–d_6) δ (ppm): 166.4, 135.8, 125.7, 102.3, 63.7, 62.6, 32.4, 26.3, 21.8, 17.9, 13.8.

2.2.2. Synthesis of 1,1′-[1,4-phenylenebis(1,3-dioxolane-2,4-diylmethylene)]-2-methyl-2-propenoic acid ester (*ArBA*)

For the synthesis of the intermediate 2,3-dihydroxypropyl-2-methyl-2-propenoic acid ester (GMA), an emulsion of glycidyl methacrylate (15.01 g, 106.0 mmol) and water (135.1 g, 7.5 mol) was heated in a 250 mL three–necked flask to 80 °C and stirred for 36 h resulting in a single–phase solution. The reaction mixture was extracted with ethyl acetate (20 × 40 mL), phenothiazine (500 ppm) were added and the solvent was evaporated under reduced pressure. GMA (16.10 g, 95% calculated yield, colorless oil) was used without further purification in the following synthetic step. n_D^{20} = 1.472. ^{1}H NMR (400 MHz, CD_3OD) δ (ppm): 6.15 (dq, *J* = 8.5, 1.3 Hz, 1H, C=CH–H), 5.63 (m, *J* = 1.6 Hz, 1H, C=CH–H), 4.85 (s, 2H, –OH), 4.22 (ddd, *J* = 11.3, 4.4, 1.3 Hz, 1H, –O–CH–H–CH), 4.14 (ddd, *J* = 11.4, 6.1, 1.3 Hz, 1H, –O–CH–H–CH), 3.87 (qd, *J* = 5.8, 4.4 Hz, 1H,–CH–OH), 3.64 – 3.52 (m, 2H,–CH–CH_2–OH), 1.95 (dq, *J* = 2.6, 1.1 Hz, 3H, –CH_3).

For the synthesis of **ArBA**, terephthalaldehyde (3.12 g, 23.3 mmol), GMA (9.91 g, 61.9 mmol), *p*TsOH (49 mg, 0.3 mmol), MEHQ (1000 ppm) and phenothiazine (300 ppm) were dissolved in 200 mL chloroform in a three–necked round bottomed flask. A reflux condenser and a Dean-Stark apparatus were attached to the round-bottomed flask, the apparatus was purged with argon and the reaction mixture was heated to reflux and stirred for four days. The solution was extracted with sat. $NaHCO_3$ solution (20 × 30 mL). The combined organic phases were dried over Na_2SO_4 and filtered, and the solvent was removed under reduced pressure. The crude product (3.3 g, 98% calculated yield, highly viscous oil) was used without further purification. n_D^{20} = 1.513. HR–MS: calc. EM + Na: 441.1520 g/mol; found: 441.1517 g/mol. ^{1}H NMR (400 MHz, DMSO–d_6) δ (ppm): 7.49 – 7.42 (m, 4H, Ar–H), 5.89 – 5.86 (m, 2H, C=CH–H), 5.78 – 5.86 (m, 4H, C=CH–H, –CH–$(O–)_2$), 4.55 – 3.93 (m, 10*H*, O=C–O–CH_2–, –O–CH_2–CH–O–, –O–CH_2–CH–O–), 1.93 – 1.88 (m, 6H, –CH_3). ^{13}C NMR (100 MHz, DMSO–d_6) δ (ppm): 166.4, 135.6, 126.7, 126.1, 103.2, 73.8, 68.2, 64.4, 17.9.

2.2.3. Synthesis of 4-(4-((methacryloyloxy)methyl)-1,3-dioxolan-2-yl) benzyl methacrylate (*ArMA*)

Three steps were necessary to synthesize the monomer **ArMA**. In the first step, 4–(4–(hydroxymethyl)-1,3-dioxolan-2-yl)benzoic acid was synthesized. Therefore, 4–formylbenzoic acid (10.00 g, 66.6 mmol), NH_4Cl (20.06 g, 375.0 mmol) and glycerol (8.18 g, 88.8 mmol) were dissolved in 200 mL chloroform in a three-necked round-bottomed flask, equipped with an inverse Dean–Stark apparatus and a reflux condenser. The apparatus was purged with argon and the reaction mixture was heated to reflux for 6 days. The precipitated product was filtered and washed with water to remove residual NH_4Cl. The product was dried at 40 °C under high vacuum and isolated as beige solid in 9.11 g (60% calculated yield) and used without further purification. m.p.: 169.2–172.1 °C. HR–MS: calc. EM + Na: 247.0577 g/mol; found: 247.0070 g/mol. ^{1}H NMR (400 MHz, DMSO–d_6) δ (ppm): 13.03 (s, 1H, –COOH), 7.97 – 7.92 (m, 2H, Ar–H), 7.58 – 7.51 (m, 2H, Ar–H), 5.61 (s, 1H, –CH–$(O)_2$, 5–membered ring), 5.41 (s, 1H, –CH–$(O)_2$, 6–membered ring), 5.25 (d, *J* = 3.1, 1H, –OH, 6–membered ring), 5.03 (d, *J* = 3.1, 1H, –OH, 5–membered ring), 4.17 – 3.90 (m, 3H, $(–O–CH_2–CH–)_2$, (–O–CH_2–CH–), 6–membered ring; (–O–CH_2–CH–), 5–membered ring), 3.79 – 3.68 (m, 1H, –OH, 5–membered ring), 3.56 – 3.50 (m, 2H, –CH_2–OH). (mixture of 5– and 6–membered rings with a ratio of 60 mol % to 40 mol%, calculated with the signals of –CH–$(O)_2$ at 5.61 ppm and 5.41 ppm. ^{13}C NMR (100 MHz, DMSO–d_6) δ (ppm): 167.1, 167.0, 143.1, 142.4, 130.99, 130.89, 129.9, 129.6, 126.42, 126.38, 99.48, 99.45, 71.67, 71.66, 71.5, 62.4, 60.2.

In the second step, the carboxylic group was reduced to a primary alcohol, to obtain (4–(4–(hydroxymethyl)1,3-dioxolan-2-yl)phenyl) methanol (**MB5**). Here, dry THF (60 mL) was placed into a three–necked flask, cooled down with an ice–bath and purged with argon for 15 min. Afterwards, $LiAlH_4$ (0.89 g, 23.5 mmol) was added in small portions to the solvent and the mixture was stirred for 10 min. A solution of **FBA5** (2.61 g, 11.6 mmol) in dry THF (100 mL) was added over a time period of 90 min with a dropping funnel to the reaction mixture without exceeding a reaction temperature of 0 °C. After complete addition, the reaction mixture was stirred for further 20 min at 0 °C and for 20 h at room temperature. An aqueous solution of KOH (2.5 wt%, 15 mL) was added to quench the excess of $LiAlH_4$. The lithium salts were filtered off, and the filtrate was washed with sat. NH_4Cl (3 × 30 mL). The combined organic phases were dried over Na_2SO_4 and filtered, and the solvent was removed under reduced pressure. The crude product was purified by recrystallization from methylene chloride to give the final product as white crystals in 3.21 g (57% calculated yield). m.p.: 76.2–79.2 °C. HR–MS: calc. EM + Na: 233.0784 g/mol; found: 233.0718 g/mol. ^{1}H NMR (400 MHz, DMSO–d_6) δ (ppm): 7.40 – 7.27 (m, 4H, Ar–H), 5.51 (s, 1H, –CH–$(O)_2$, 5–membered ring), 5.39 (s, 1H, –CH–$(O)_2$, 6–membered ring), 4.49 – 4.48 (m, 2H, Ar–CH_2–OH), 4.13 – 4.10 (dd, *J* = 10.8, 5.3 Hz, 1H, –O–CH–CH_2–OH), 4.03 and 3.93 (d, *J* = 6.7 Hz, 4H, –O–CH_2–$CHCH_2$–O–, –O–CH_2–CH–CH_2–OH), 3.74 – 3.66 (m, 1H, –O–CH_2–CH–CH_2–O), 3.50 – 3.26 (m, 2H, –O–CH–CH_2–OH). (mixture of 5– and 6–membered rings with a ratio of 60 mol% to 40 mol%, calculated with the signals of –CH–$(O)_2$ at 5.51 ppm and 5.38 ppm). ^{13}C NMR (100 MHz, DMSO–d_6) δ (ppm): 142.9, 142.8, 137.3, 136.5, 125.95, 125.89, 125.88, 125.82, 100.21, 100.19, 71.6, 71.4, 62.61, 62.57, 62.4, 60.2.

In the last step of the synthesis for **ArMA**, photopolymerizable groups were attached. Therefore, **MB5** (1.7 g, 8.1 mmol), MEHQ (1000 ppm), phenothiazine (300 ppm) and triethylamine (2.46 g, 24.3 mmol) were dissolved in dry THF (200 mL), cooled with an ice bath in a three–necked round bottomed flask and purged with argon. Freshly distilled methacryloyl chloride (2.03 g, 19.4 mmol) was diluted in 20 mL dry THF and added dropwise to the reaction mixture. The reaction mixture was stirred for 1 h at 0 °C. Then, the reaction mixture was stirred for additional 2 days at room temperature. The reaction mixture was filtered to remove salts and washed with THF. The organic layer was washed with sat. NH_4Cl (3 × 30 mL) and brine (2 × 20 mL). The combined organic phases were dried with Na_2SO_4, filtered and the solvent was removed under reduced pressure. The product was recrystallized in methylene chloride and was isolated as yellow crystals in 2.6 g (91% calculated yield). m.p.: 66.8 – 73.2 °C. ^{1}H NMR (400 MHz, DMSO–d_6) δ (ppm): 7.45 – 7.35 (m, 4H, Ar–H), 6.06 (s, 2H, CH_2=), 5.75 – 5.74 and 5.71 – 5.69 (m, 2H, CH_2=), 5.59 (s, 1H, –CH–$(O)_2$, 5–membered ring), 5.42 (s, 1H, CH–$(O)_2$, 6–membered ring), 5.22 – 5.17 (m, 2H, Ar–CH_2–O), 4.92 – 4.84 (m, 1H, –O–CH_2–CH–CH_2–O–), 4.33 – 4.29 (m, 1H, –O–CH–CH_2–O–), 4.15 – 4.10 (m, 2H, –O–CH_2–CH–O–), 3.81 – 3.67 (m, 2H, –O–CH_2–CH–), 3.50 – 3.45 (m, 2H,–O–CH–CH_2–O–), 1.90 – 1.88 (m, 6H, –CH_3). (mixture of 5– and 6–membered rings with a ratio of 40 mol% to 60 mol%, calculated with the signals of –CH–$(O)_2$ at 5.60 ppm and 5.42 ppm). ^{13}C NMR (100 MHz, DMSO–d_6) δ (ppm): 166.3, 156.6, 137.9, 137.3, 136.9, 136.6, 137.7, 135.3, 127.5, 127.4, 126.7, 126.31, 126.29, 126.10, 126.07, 100.1, 99.9, 71.6, 67.6, 65.49, 65.46, 62.8, 60.2, 17.99, 17.85.

2.2.4. Characterization

Formulation and Specimen Preparation. The preparation of resin formulations was performed in an orange light laboratory to avoid unintended polymerization. The laboratory windows were equipped with adhesive foils purchased from the company IFOHA. The foil filters wavelengths below 480 nm. Fluorescent lamps from Osram luminux with chip control light color 62 were used. The germanium–based photoinitiator (PI) Ivocerin® (1 mol%) with a maximum absorption at 408 nm, the corresponding monomers and the reactive diluent *N*–acryloylmorpholine (NAM) were weighed into a brown glass vial. The formulations were mixed with a vortex speed mixer for about one minute and left in an ultrasonic bath for additional 5 min.

Specimen with a geometric shape of 2 × 5 × 40 mm^3 for the thermomechanical measurements (DMTA) and network degradation studies were photocured in a Lumamat 100 light oven (provided by Ivoclar Vivadent) (400–500 nm) with 6 Osram Dulux L Blue 18 W lamps. Exposure was performed for 10 min on the top and additionally 10 min on the backside of the samples.

RT-FTNIR-Photorheology. RT–FTNIR-Photorheology measurements were conducted on an *Anton Paar MCR 302 WESP*. A P–PTD 200/GL Peltier glass plate and a PP25 measuring system were used. A FTIR spectrometer (*Bruker Vertex 80*) with external mirrors to guide the IR beam through the sample during the rheology measurements, was coupled with the rheometer to analyze the double bond conversion over time. More details about the setup and the measurements can be found in literature [45]. For detection of the reflected beam, a MCT–detector was used. The measurements were performed in triplicates at room temperature (25 °C). 150 µL sample volume was applied on a glass disk which was covered with a PE tape. The PE tape is necessary to remove the samples after irradiation easily. The gap size between the measuring system and the glass plate was set to 200 µm. UV curing was done with an *Omnicure Series 200 EXFO* as a light source with a 200 W Hg lamp and an installed filter (wavelength of 400–500 nm). The light intensity at the surface of the PE tape (attached to the glass plate) was measured by an *Ocean Optics* USB 2000 + spectrometer and set to 10 mW cm^{-2}. The samples were irradiated for 300 s. The photorheology measurements were analyzed with the software Rheoplus V3.62 from *Anton Paar,* and the IR spectra were analyzed with the software Opus 7.0 from *Bruker*. Due to the simultaneously measured NIR spectra, the double bond conversions (DBC) can be calculated from the reduction of the integrated peak area of the double bonds of (meth)acrylates at about 6170 cm^{-1} wavenumbers.

Dynamic Mechanical Thermal Analysis (DMTA). DMTA measurements were performed with an Anton Paar MCR 301 device with a CTD 450 oven and an SRF 12 measuring system. One specimen *per* formulation was tested in torsion mode with a frequency of 1 Hz and a strain of 0.1%. A temperature interval from –100 to 200 °C was chosen with a heating rate of 2 °C min^{-1}. The temperature at the maximum dissipation factor (tan δ) was defined as the glass transition temperature T_g.

Degradation Experiments. The model degradation study of low molar mass acetals was performed with ^{1}H NMR spectroscopy. Therefore, monomers were dissolved in a 1:1 mixture of CD_3CN/D_2O. Then, 0.5 µL deuterated hydrochloric acid (DCl) were added, and the samples were measured immediately and every hour to monitor the degradation.

Swelling and degradation behavior experiments were performed with photopolymerized DMTA specimens. These samples have a defined shape of (2 × 5 × 13 mm^2), thus reproducible geometry. The samples were weighed ($m_{0,dry}$) and stored in 15 mL acidic solution (hydrochloric acid – potassium chloride solution with a set pH = 2.2) at a constant temperature of 37 °C. The hydrochloric acid – potassium chloride solution was prepared by mixing 7.45 g of KCl, 772 mg of HCl with 1 L of distilled water. All degradation experiments were conducted in triplicates. The pH value was monitored every 3 days to ensure that the pH is constant, and the acidic solution was renewed once a week. In order to determine the mass change, the samples were taken from the solution ($m_{t,swollen}$), dried using a paper towel, weighed, and placed into the acidic solution again. The mass change of the polymer networks was determined as follows:

$$Mass\ \ change[\%] = \frac{m_{t,swollen} - m_{0,dry}}{m_{0,dry}} \cdot 100$$

3. Results and discussion

3.1. Monomer synthesis

Acetals is the general term for products obtained from the reaction of a carbonyl compound with two hydroxyl functionalities. The carbonyl compound can either be an aldehyde or a ketone. In some cases, products derived from ketones are referred to as ketals. For the discussion concerning the stability against hydrolysis these two types of acetals must be differentiated. Acetals formed from ketones are more sensitive to hydrolysis in comparison to acetals from aldehydes. Further, the degree of substitution at the central carbon of an acetal has a great impact on the hydrolysis rate. In general, a higher degree of substitution increases the hydrolysis rate, thus, the relative rate follows the order: formaldehyde < aldehyde < ketone [46–48]. The degradation of linear acetals is more entropically favored than the degradation of their cyclic counterparts [49–51]. Further, the ring size substantially affects the hydrolysis rate for cyclic acetals. A 5–membered ring with the same substituents as a 6–membered ring is more stable [47]. For this study, we designed three different acetals and synthesized them intending to investigate their degradation behavior. Linear acetals exhibit greater flexibility, whereas cyclic acetals are more rigid. Hence, an aliphatic and linear acetal 1,1′-[pentanebis(oxy-2,1-ethanediyl)]-2-methyl-2-propenoic acid ester (**AlLA** (see Scheme 1)) as well as the aromatic cyclic acetals 1,1′–[1,4–phenylenebis(1,3-dioxolane-2,4-diylmethylene)]-2-methyl-2-propenoic acid ester (**ArBA** (see Scheme 1)) and 4-(4-((methacryloyloxy)methyl)-1,3-dioxolan-2-yl)benzyl methacrylate (**ArMA** (see Scheme 1)) were synthesized. The influence of the different acetal structures on the mechanical properties and the degradation characteristics in polymeric networks was of interest. Hence, the acetal–based molecules were functionalized with photopolymerizable moieties.

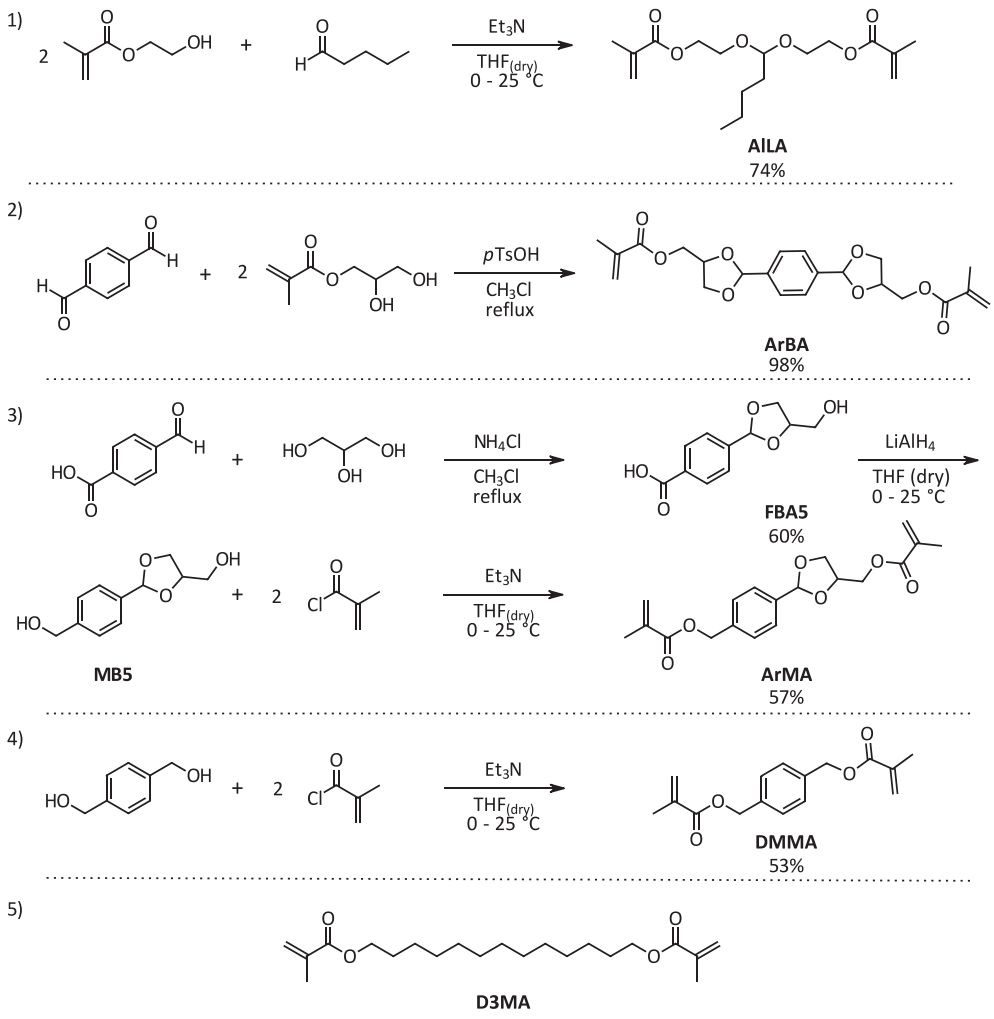

Scheme 1. Synthesis and chemical structures of the synthesized acetals **AlLA (1), ArBA (2), ArMA (3),** and the commercially available non-degradable reference precursors **DMMA (4)** and **D3MA (5)**.

Methacrylates were chosen for photopolymerization as they are easily accessible, commonly used [52] and considered to have a sufficient biocompatibility [53,54]. In addition, a model compound (**EIBSPG**) was synthesized as the acetal–based reference system (more details are available in the SI). This molecule contains a spiroacetal moiety, which is known for its stability under acidic conditions [44] as well as an ester moiety. This ester group is also included in the reference system in order to make a direct comparison between acidic degradable acetals and commonly used esters. Moreover, two reference systems (aliphatic **D3MA** and aromatic **DMMA** (see Scheme 1) and details in SI) were used as non-degradable precursors.

In general, the acetal-based monomers were synthesized in condensation reactions of the corresponding carbonyl compounds with the respective alcohols using *p*–toluenesulfonic acid as an acidic catalyst [55]. The linear and aliphatic acetal was synthesized using valeraldehyde and hydroxyethyl methacrylate (HEMA) as starting materials. Aldehydes are generally known as toxic compounds due to their high reactivity. As an example, aldehydes can couple with free amino groups of proteins leading to denaturation. The toxicity of linear aldehydes decreases with increasing chain length. Furthermore, saturated aldehydes are more biocompatible than unsaturated ones [34]. Taking these points into consideration, valeraldehyde was chosen as a starting material, as it has a long and unsaturated aliphatic chain and thus has a low toxicity. The monofunctional alcohol HEMA was chosen, since it is known as a suitable biocompatible material [56] for medical applications [57,58]. In addition, the acetal moiety was introduced in a simultaneous step as the photopolymerizable group.

Synthesis of a bicyclic aromatic acetal requires a difunctional aldehyde as starting material. Therefore, terephthalaldehyde was chosen, as it is also considered harmless [59]. Glycerol methacrylate (GlyMA) functions as source for the difunctional alcohol glycidyl methacrylate (GMA). According to Ratcliffe *et al* [60] a ring opening reaction of the epoxy group of GlyMA was carried out to obtain two hydroxyl groups in one molecule. The reaction of the difunctional alcohol with the difunctional aldehyde lead to the bicyclic aromatic acetal **ArBA**. During the ring-opening reaction of GlyMA an intramolecular rearrangement occurs, leading to a minor formation of the side product 2-hydroxy-1-(hydroxymethyl)ethyl-2-methyl-2-propenoic acid ester [60]. For this reason, a mixture of 5– and 6– membered acetals are obtained during the conversion with terephthalaldehyde. However, as the 5–membered rings were formed in larger quantities, only this product will be depicted in the following text.

The aromatic monocyclic acetal **ArMA** was synthesized in a three-step procedure. 4–Formylbenzoic acid was selected as starting material due to the electron-withdrawing carboxylic acid, which further accelerates the acetal formation with glycerol. Here, 5– and 6–membered cyclic acetals were formed as well. The 5–membered ring is kinetically favorable (more stable) and thus formed in larger quantities. Hence, only this product will be depicted in the following text. Then, the carboxylic acid can be reduced to the corresponding primary alcohol, which is necessary for further functionalization. Furthermore, this newly formed primary alcohol group makes the product more flexible.

The synthesized diol was esterified by converting its hydroxyl groups with methacryloylchloride and thus the photopolymerizable groups could be attached.

3.2. Investigation of network formation with RT-FTNIR-photorheology

RT–FTNIR-Photorhology is an elegant and efficient tool to determine the material properties and the corresponding double bond conversion *in situ, i.e.* during photopolymerization. Through this method, mechanical data is directly linked with molecular information. The different parameters obtained during these measurements (time until 95% of the final double bond conversion (DBC_{final}) is reached (t_{95}), final DBC (DBC_{final}), final shrinkage stress (normal force, $F_{N,final}$), final storage modulus (G'_{final}), enable a rational assessment of the photopolymerization process. Difunctional and multifunctional methacrylates, are used in several industrial areas *e.g.*, dental composites or additive manufacturing technologies (AMT), respectively. The main disadvantages are the developed shrinkage stress and the brittleness of the final material. These disadvantages of dimethacrylates result from the rapid formation of an extremely dense polymer matrix due to a high number of cross-links [45,61]. To counterbalance these drawbacks, the reactive diluent *N*–acryloylmorpholine (NAM) was used in a 1:4 double bond ratio (DB ratio) with four double bond parts of the monomer NAM to decrease network density while maintaining good mechanical properties (high toughness, high T_g) and good rheological behavior (low viscosity).

For photorheological tests, mixtures of the acetal-based monomers and NAM were prepared, and 1 mol% of Ivocerin® was added as a photoinitiator. The photoreactivity of the prepared formulations was assessed *via* RT–FTNIR-photorheology at 25 °C with a UV/vis broadband light source combined with a wavelength filter (400–500 nm). The irradiation of formulations in this visible light range shows benefits for the future application as bone replacement material. Ivocerin® was chosen as PI as it shows low cytotoxicity and intense absorption in the visible region and is already used for tissue engineering applications and dental fillings [62]. Further, Ivocerin® shows rapid curing with increased curing depth even in highly filled systems, which is important for 3D printing [63]. The time until 95% of the final double bond conversion is reached (t_{95}) is in case of all formulation relatively fast (51 s – 72 s) (see Table 1). This fast performance of all formulations is a crucial parameter for a successful 3D printing process. The final double bond conversions (DBC_{final}) are comparable for all formulations (86% – 95%) and could be calculated from the integrated peak area of the double bonds of (meth)acrylates at ~ 6170 cm^{-1}. The same observations were made for the final shrinkage stress (normal force, $F_{N,final}$) and the final storage modulus G'_{final}. These comparable results can be explained by the high content of the reactive diluent NAM in all formulations. Because of the high amount of reactive diluent, all materials perform comparably in the formation of the photopolymer networks.

Table 1
RT-FTNIR-Photorheology results for the photopolymerization of **D3MA**, **AlLA**, **DMMA**, **ArMA** and **ArBA** (all formulations containing NAM in a 1:4 DB–ratio and 1 mol% PI).

Formulation	t_{95} [s]	DBC_{final} [%]*	$F_{N,final}$ [N]	G'_{final} [MPa]*
D3MA	51 ± 2	95	−24.3 ± 0.1	0.63
AlLA	54 ± 7	93	−24.1 ± 0.3	0.66
DMMA	60 ± 3	93	−24.4 ± 0.1	0.61
ArMA	54 ± 3	94	−23.8 ± 0.2	0.61
ArBA	72 ± 3	86	−23.4 ± 0.6	0.66

t_{95} = time until 95% of the final double bond conversion DBC_{final} is reached; DBC_{final} = final double bond conversion; $F_{N,final}$ = final shrinkage stress; G'_{final} = final storage modulus. *DBC final calculated from the peak area at ~6170 cm^{-1}. The standard deviation for the final double bond conversion is lower than ±0.3%. The standard deviation for the final storage modulus is always lower than ±0.01 MPa.

3.3. Dynamic mechanical thermal analysis (DMTA)

Valuable information on the crosslinking and its underlying processes were obtained by photorheology measurements. The final thermomechanical properties of the material are affected by the change of the network architecture, which needs to be characterized by dynamic mechanical thermal analysis (DMTA). DMTA provides the impact of the acetal–based monomers on the thermomechanical properties of the polymer network. This method was used to obtain the storage modulus (G') at different temperatures and to determine the glass transition temperatures (T_g), from the maximum of the loss factor (tan δ). A rather broad glass transition (full width at half maximum of tan δ, FWHM) indicates an unregulated polymer network. The storage modulus at the rubber plateau (G'_R) correlates with the degree of network crosslinking. A high G'_R is indicative for a highly cross–linked network [61,64].

The aliphatic reference system **D3MA** and the aliphatic linear acetal **AlLA** show no significant difference in their thermomechanical properties (see Table 2). Aromatic systems show a higher glass transition temperature due to steric effects. π–Stacking leads to a decrease in the chain mobility, hence an increase of the T_g. The reference system **DMMA** shows the highest T_g and the highest storage modulus at the rubber plateau (G'_R), which could be reasoned by the high monomer symmetry that might promote π–stacking. The acetal moieties lead to a higher flexibility and a decreased T_g. Indeed, the two acetal moieties of **ArBA** induce a much sharper glass transition (FWHM) with a significantly lower T_g and a lower storage modulus at the rubber plateau (G'_R). These values are distinctive for a regulated network and therefore, a more homogenous and less cross–linked network is assumed. A low crosslink density is expected for **ArMA** as it shows the lowest G'_R. This could be explained by reduced π–stacking due to the mixture of 5– and 6–membered rings, which might lead to more unregular polymer structure.

The different storage moduli G' obtained *via* RT–FTNIR-photorheology and *via* DMTA measurements are not comparable. In the RT–FTNIR-photorheology measurements, values of about 600 kPa were obtained. When interpreting these values, it should be taken into consideration that PE tape had to be used during the measurement which influenced these values. Storage moduli measured *via* DMTA were obtained by torsion deformation and were above 1 GPa. In literature values between 3 and 9 GPa are described for bones, depending on the frequency of the measurement and water content [65]. However, the Young's modulus (E') is more commonly reported in literature as a characterization parameter for the stiffness of bones. Here, values for cortical bones, which are approximately 7 – 30 GPa and 0.05 – 0.5 GPa for cancellous bone, can be found [66]. Nevertheless, the glass transition temperatures of all acetal-based specimens exceed the human body temperature of approximately 37 °C. This is a viable parameter to evaluate their applicability as bone replacement material, as the material should not soften or deform in the body.

Table 2
Results from DMTA measurements of photopolymerized specimens; formulation contained the reference system/acetal–based monomer and NAM (1:4 DB-ratio), and 1 mol% PI.

Formulation	T_g [°C]	G'_{25} [MPa]	G'_{37} [MPa]	G'_R [MPa]	FWHM [°C]
D3MA	151	1487	1432	8.8	30.1
AlLA	148	1899	1820	7.1	29.9
DMMA	180	1770	1712	14.4	41.0
ArMA	156	1984	1897	3.9	35.7
ArBA	168	2154	2100	7.1	21.5

T_g = glass transition temperature; $G'_{25/37}$ = storage modulus at 25 °C and 37 °C; G'_R = storage modulus at the rubber plateau; FWHM = full width at half maximum of tan δ.

3.4. Degradation experiments

Commonly used biomaterials are based on polyester, which lead to acidic degradation products after hydrolysis, potentially harming surroundings and inducing inflammatory responses. Furthermore, the hydrolysis of polyester is slower in acidic environments, which is demanded for some applications. As an example, grafts for bone replacements can be mentioned. During the process of osteoclast–driven bone resorption, an acidic environment with a pH value below 3 is created [16,21,22]. The degradation process for acetal-based biomaterials *in vivo* is usually a hydrolytic process, which can be catalyzed by enzymes [67,68]. In order to determine the hydrolysis stability of the acetal–based monomers, the degradation experiments were run under acidic aqueous conditions. **AlLA**, **ArBA,** and **ArMA** are based on linear and cyclic acetals as cleavable moieties. The degradation of acetals leads to the release of alcohols and carbonyls and, therefore, avoids acidic degradation products. These primary degradation products are expected not to affect local acidity and do not induce inflammatory reactions in the human body [37,39]. The degradation of these linear and cyclic acetals had to be studied in order to assess their potential for polymer–based biomaterials in tissue engineering. For this purpose, model degradation studies of the molecules for direct comparison of their stability against hydrolysis were conducted. This model studies only assess the cleavage of the chemical moiety, but the polymer matrix's degradation behavior can differ due to matrix effects. In this case, degradation of the polymer also depends on chain mobility and crystallinity [69,70]. Therefore, in addition to molecular degradation studies, their behavior in polymeric networks was investigated. However, it must be considered that the presented *in vitro* experiments are not comparable to an *in vivo* study.

3.5. Molecular model degradation study of acetal–based monomers

For the model degradation study of low molar mass acetals, ^{1}H NMR spectroscopy was chosen and the experiments were performed at room temperature. The samples were dissolved in a D_2O/CD_3CN mixture (0.7 mL) and by addition of 0.5 μL DCl an acidic environment is created, which is equivalent to a pH value of about 2.1. Increase or decrease of characteristic signals was followed over time and the residual molar ratio of the acetals was plotted against the time.

Fig. 1 shows the hydrolytic degradation of the aliphatic acetal **AlLA** expected for acidic conditions and the residual molar ratio of acetal (in [mol%]) over time. For this purpose, the methylene proton signal (6.67 ppm) was used as an internal standard and the decay of the acetal proton (5.23 ppm) was taken as measure for the degradation. The NMR spectra for determining the residual acetal **AlLA** are illustrated in the Supporting Information (Fig. S. 7). The experiments show that within the first 6 h, half of the acetal is cleaved, and after 2 days, the acetal can be considered fully degraded. The detailed ^{1}H NMR spectra are depicted.

The degradation study of the aromatic bicyclic acetal **ArBA** shows two cleavage steps. It can be cleaved on one side or both sides under acidic conditions. This mechanism is shown in Fig. 2. For calculation of the amounts of one-side cleaved and two-side cleaved acetals, the signals of the protons on the aromatic ring (**ArBA**, 8.12 ppm) were used as an internal standard as other characteristic signals were not isolated and overlapped. After degradation of the first acetal, the signals separate (8.22 and 8.50 ppm). If both acetals are completely cleaved, terephthalaldehyde is formed and the aromatic protons collapse again to a singlet at 8.65 ppm. The aromatic proton signals of the respective degradation products were used as measure for degradation.

Fig. 2 shows the illustration of the degradation process of the starting material **ArBA**. If the cleavage of one acetal moiety per molecule occurs, the molecule **ArBA** is considered degraded, as this would also directly lead to the cleavage of network meshes. According to this definition, the

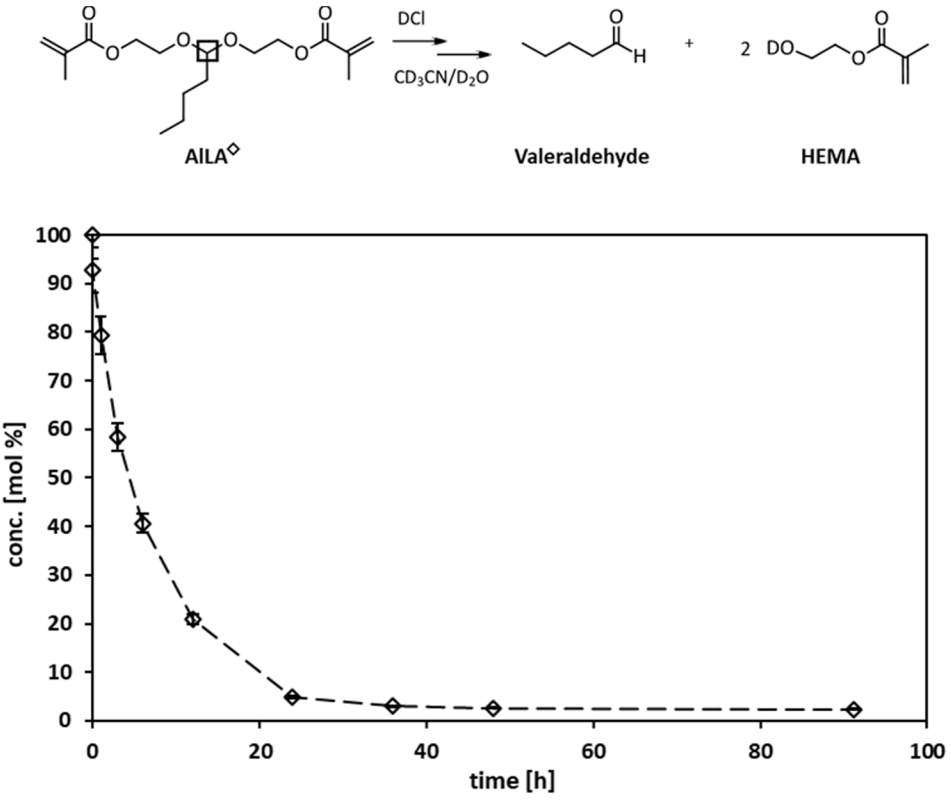

Fig. 1. Degradation scheme and process of **AlLA** (–◇–) under acidic conditions by deuterated hydrochloric acid (pH-equivalent of 2.1) during 80 h. (Degradation products: Valeraldehyde and HEMA) For better visibility, the symbols were connected with straight lines.)

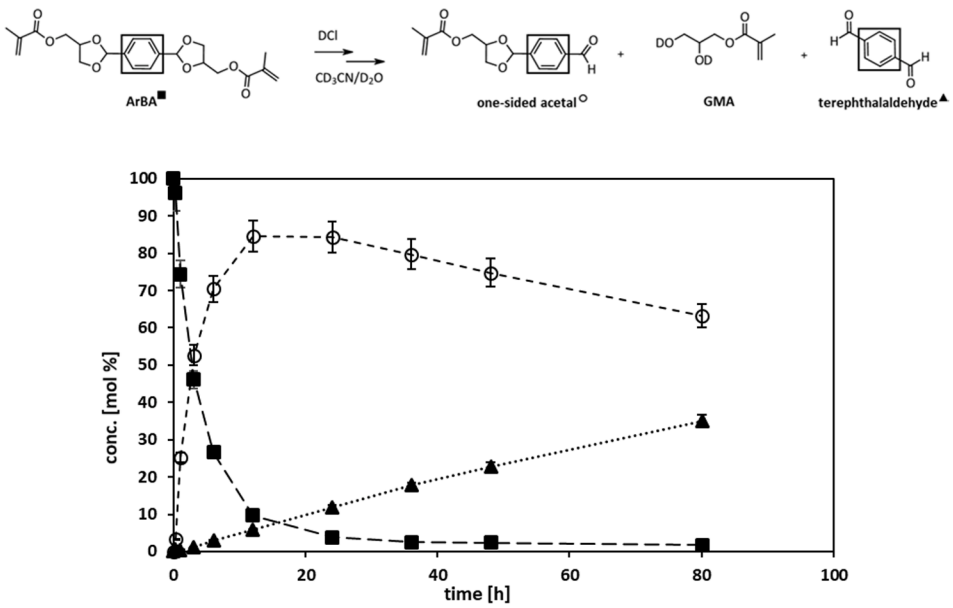

Fig. 2. Degradation scheme and process of **ArBA** (–■–) under acidic conditions by deuterated hydrochloric acid (pH-equivalent of 2.1) during 80 h. (Degradation products: one–sided acetal (–○–), terephthalaldehyde (··▲··)) For better visibility, the symbols were connected with straight lines.)

product is already degraded after one day. Consideration of the degradation process in detail shows that about 80 mol% of the single–side–cleaved product is formed within the first 10 h. Afterwards, the cleavage of the second acetal sets in and the amount of the single–side–cleaved product decreases again. Due to the formation and degradation of this intermediate product, the curve of the formation of terephthalaldehyde ascends steadily. The NMR spectra for the determination of the residual acetal **ArBA** and the degradation products, respectively, are illustrated in the Supporting Information (Fig. S. 8).

For the degradation experiment of the monocyclic aromatic acetal, it must be stressed again that this is a mixture of 5– and 6–membered rings. The degradation of the monocyclic aromatic acetal (5– and 6–membered ring) under acidic conditions and the residual mol% acetal in total and for the respective rings are shown in Fig. 3.

The signals of the aromatic protons (8.07–7.90 ppm) were used as internal standard to determine the degradation by ^{1}H NMR spectroscopy. With this standard and the acetal protons (6.17 ppm for the 5–membered ring, 6.04 ppm for the 6–membered ring), the amount of 5– and 6–membered rings was calculated. In the beginning, it was determined that the 5–membered ring was formed to 60 mol%. It is

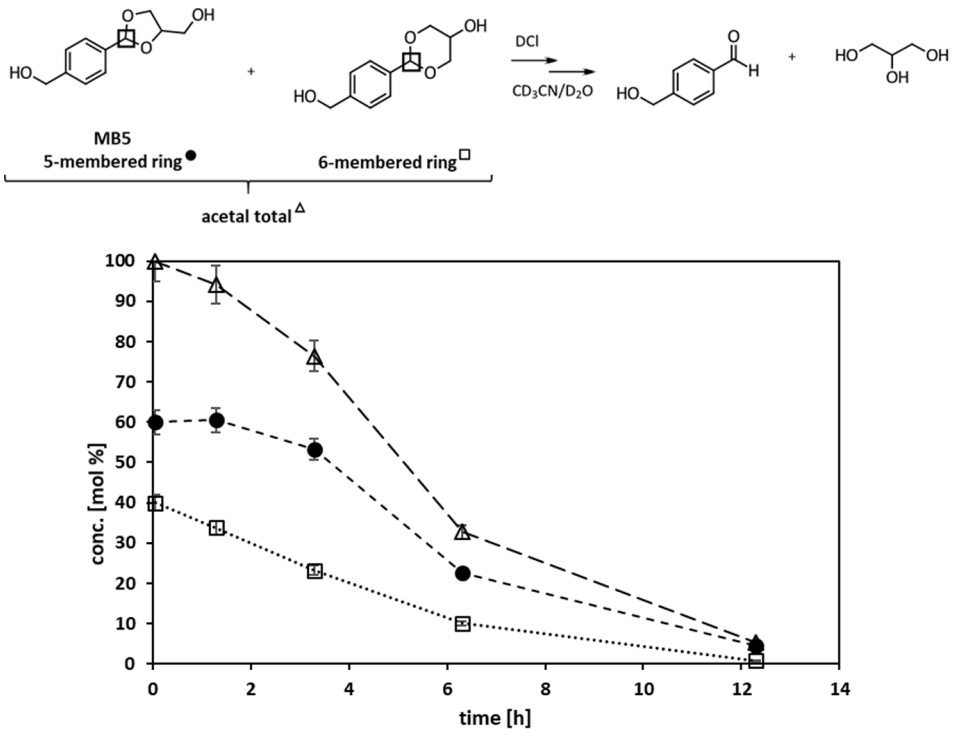

Fig. 3. Degradation scheme and process of monocyclic aromatic acetal (–△–) under acidic conditions by deuterated hydrochloric acid (pH–equivalent of 2.1) during 14 h. (5–membered ring: –●–, 6–membered ring ··□··) For better visibility, the symbols were connected with straight lines.)

assumed that the 6–membered ring is more unstable as it was also formed in smaller amounts. This can also be seen in the degradation behavior, as it cleaves much faster than the 5–membered acetal. During the degradation study, it was shown that both acetals were almost completely degraded within 12 h. All NMR spectra of the monocyclic aromatic acetal are shown in the Supporting Information (Fig. S.9).

In case of cyclic acetals, ring strain is not the major factor contributing to the thermodynamic stability [71]. Instead the thermodynamic stability and thus the hydrolysis rates are determined by stereo electronic effects resulting from the most stable chair conformation of the six-membered acetal ring [72]. In this conformation the equatorial lone pair orbital is aligned with, and thus is donating electron density into the antibonding σ*–orbital of the dissociating C—O bond [72]. It is important to point out, that the hydrolysis rate of cyclic acetals is also dependent on the substituents and to some extend also on the ring strain.

A small spiroacetal model molecule (EIBSPG, SI) was employed for a better comparison of acetal–based molecules with ester-based materials. Spiroacetals are commercially available and stable under acidic conditions [44]. This experiment proved the stability of the spiroacetal moiety and showed the slow cleavage of the ester group in the acidic environment (the detailed study can be found in SI, Fig. S.5–6).

The first three hours of the degradation experiments were studied in detail to better compare the three different monomers with each other and to compare them with the stable spiroacetals and commonly used esters (Fig. 4). The degradation was fitted linearly and thus, the parameter mol% degradation per hour [mol%/h] was calculated. This resulted in a degradation rate of 18 mol%/h for the bicyclic acetal **ArBA**, which corresponds to the fastest cleavage than the other acetals. Again, it was defined that the acetal is considered degraded as soon as one of the two acetal groups is cleaved. This is followed by the linear acetal **AlLA** with 13 mol%/h. **ArMA** proved to be the most stable of the three acetals. This monocyclic acetal degrades at a rate of 8 mol%/h. If the mixture of 5– and 6–membered rings is considered separately, the 6–membered ring cleaves at 12.5 mol%/h and the smaller ring at 5 mol %/h. With the determination of the degradation rate, the stability of varying acetals structures described in literature can be proved. The degradation of linear acetals is typically faster than cyclic acetals [49–51]. However, **ArBA** is an exception, as the substituents on the benzene ring in para position to the acetal group have a very important influence [48] and hence, lead to lower stability. Further, the ring size has an important impact on the hydrolysis rate for cyclic acetals. A 6–membered ring with the identical substituents as a 5–membered ring is less stable [47].

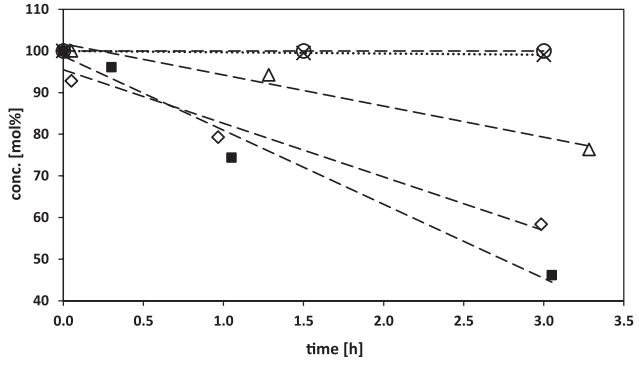

Fig. 4. Detailed view on the degradation experiments for **EIBSPG** (spiroacetal moiety (–○–)) and ester moiety (··X··)), for monocyclic aromatic acetal **MB5** (–△–), for **AlLA** (–◇–) and for the **ArBA** (–■–) under acidic conditions by deuterated hydrochloric acid (pH-equivalent of 2.1) within the first three hours. (For better visibility of the degradation speed, a trendline is used.)

3.6. Swelling and degradation behavior of polymer networks

Molecular degradation studies only provide an insight into the degradability of individual molecules and their functional groups, respectively. In order to investigate the degradation as a polymer network and determine the matrix effects of the polymerized material, swelling and mass loss tests were performed. Strictly speaking, swelling of polymer networks is defined as volumetric change, which was also observed during the experiments (Fig. 5a). But here, an increase in mass due to water uptake was taken as indication for swelling. Degradation, which corresponds to cleavage of the polymer chains and thus formation of oligomers and other small molecules, and loss were differentiated. Mass loss describes the loss of material caused by washing–out oligomers and monomers from the network due to degradation [73,74].

Different processes are expected during the degradation of polymer networks. As soon as the network starts to degrade, further expansion of the network is expected, leading to higher water uptake and a further increase in mass. Consequently, an even more frequent cleavage of labile bonds is hypothesized and would lead to elution of small fragments from the network, and thus a mass loss can be observed [69]. These processes would be determined as mass changes over time. Water uptake would correspond to a positive mass change and mass loss to a negative mass change. However, especially at the beginning of the degradation process, mass loss is supposed to be overcompensated by the water uptake and therefore, only a positive mass change would be observable.

For the determination of the degradation behavior, photopolymerized specimens were prepared. For this purpose, difunctional acetal-based monomers (**AlLA**, **ArBA** and **ArMA**), as well as the reference monomers (**D3MA** and **DMMA**) were mixed with NAM in a 1:4 DB-ratio (monomer:NAM) and 1 mol% PI (Ivocerin®) were added. These prepared formulations were photopolymerized and immersed in an acidic solution with a set pH value of 2.2. The samples were stored at 37 °C and weighed at regular intervals.

Fig. 5b shows the positive mass change and the mass loss, respectively, of the different acetal–based specimen and their reference systems. The non–degradable reference systems based on ester moieties as single functional groups show a slight increase in mass (about 20%) due to water uptake. Still, afterwards the weight of the samples stays constant over the whole period. This change in mass until the equilibrium swelling is reached and the stable weight indicates a non–degradable system. All acetal-based systems, however, show a steady increase in their mass. During the studies, the mechanical properties were changing due to the swelling process (Fig. 5a). A softening effect was observed for all acetal–based photopolymerized specimens. However, photopolymers based on **AlLA** show a mass change of 700% in the first week, but then, the samples disintegrate and the experiment had to be terminated for this material. The aromatic systems (**ArBA** and **ArMA**) are more rigid than the aliphatic one (**AlLA**), which shows impact on the matrix effect and hence, the water–uptake. Therefore, the swelling takes more time than for the aliphatic one. Nevertheless, there is a difference between the two polymer networks based on aromatic cyclic acetals. The polymeric network based on the monocyclic acetal **ArMA** shows 140% swelling within the first week and herewith significantly less swelling than the polymer network of the bicyclic system **ArBA**. Here, up to 200% mass change is reached in one week and the mass change increases steadily. Considering the degradation model studies of the two monomers, it was found that the bicyclic systems are cleaved faster, which could also explain the widening of the network and therefore, a higher water-uptake. Nevertheless, after 25 days, the photopolymer network of the monocyclic **ArMA** shows a decrease in mass, indicating that the mass loss overcompensates the swelling. To differentiate between the degradation due to swelling and the actual mass loss, the samples have to be dried. Thus, at least one sample was taken from the buffer solution and dried at 50 °C in an oven until no change in weight could be measured. The photopolymer networks based on the reference systems **D3MA** and **DMMA** show a mass loss of 8% and 6%, respectively, compared to their

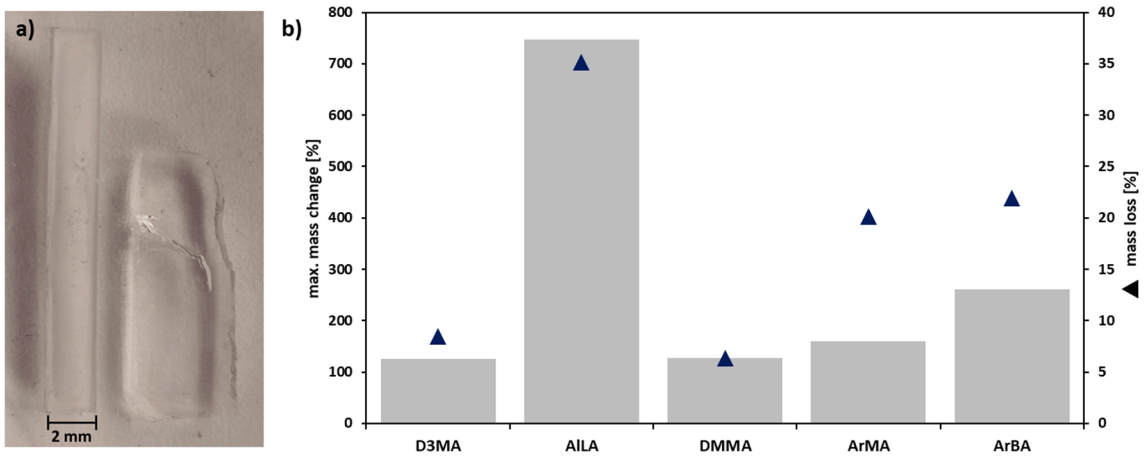

Fig. 5. a) Photopolymerized specimens based on the difunctional acetal AlLA before and after 5 days of immersing in a HCl/KCl solution with a pH value of 2.2. b) The maximum of the water uptake (max. mass change [%]) as columns) and the mass loss after constant drying (as diamond) compared to their initial mass for the aliphatic reference system D3MA (within 246 days), AlLA (within 5 days), the aromatic reference system DMMA, ArMA (both within 246 days) and ArBA (within 233 days).

initial mass. The polymerized network based on the linear aliphatic acetal **AlLA** shows a mass loss of 35% (±3%). In this case, all three samples were dried due to a rapid degradation during swelling. The photopolymerized aromatic acetal-based systems also show a significant mass loss. The mass of **ArMA** is 20% lower than its initial mass and the mass of **ArBA** decreased 21% in about eight months. In conclusion, all acetal–based photopolymer network showed a significantly higher mass loss than the reference systems. The change in their mechanical properties, the volumetric change and their behavior in these swelling and degradation experiments argues for a bulk degradation, which was expected due to the hydrophilic character of the polymer networks.

4. Conclusion

New degradable photopolymerizable precursors, containing linear and cyclic acetals as acid labile moieties have been synthesized as possible alternatives to esters for biomaterials in TE. The polymer network formation was studied by RT–FTNIR-photorheology. High reactivity and double bond conversion were found for the synthesized monomers, which are requirements for a rapid 3D printing process. The obtained photopolymers have desired properties such as high glass transition temperature and high storage moduli, which were determined by dynamic mechanical thermal analysis. A T_g above the body temperature is crucial for the possible application as bone replacement materials and all photopolymers have fulfilled this criterion. In molecular degradation studies carried out through ^{1}H NMR spectroscopy it could be shown that all alternative (linear and cyclic) acetals degrade faster by a factor of 80–200 when compared to corresponding ester moieties. An additional network degradation study with the photopolymerized samples could show a higher swelling and mass loss in all acetal-based samples compared to the reference systems. Therefore, acetals can be added to the toolbox of cleavable moieties for an acidic environment in TE.

CRediT authorship contribution statement

Barbara Dellago: Validation, Formal analysis, Data curation, Investigation, Writing - original draft, Visualization. **Alexander Ricke:** Validation, Formal analysis, Data curation, Investigation, Writing - original draft, Visualization. **Theresa Geyer:** Validation, Formal analysis, Investigation. **Robert Liska:** Conceptualization, Writing - review & editing, Supervision, Funding acquisition. **Stefan Baudis:** Conceptualization, Writing - review & editing, Supervision, Project administration, Funding acquisition.

Declaration of Competing Interest

The authors declare that they have no known competing financial interests or personal relationships that could have appeared to influence the work reported in this paper.

Acknowledgement

Funding by the Christian Doppler Research Association within the framework of the "Christian Doppler Laboratory for Advanced Polymers for Biomaterials and 3D Printing" and the financial support by the Austrian Federal Ministry for Digital and Economic Affairs and the National foundation for Research, Technology and Development are gratefully acknowledged. This project has received funding from the European Union's Horizon 2020 research and innovation program under the Marie Skłodowska-Curie grant agreement no. 765341 (Project PHOTO-EMULSION, MSCA-ITN-2017). The authors acknowledge TU Wien Bibliothek for financial support through its Open Access Funding Programme.

Data availability

The raw/processed data required to reproduce these findings cannot be shared at this time as the data also forms part of an ongoing study.

Appendix A. Supplementary material

Supplementary data to this article can be found online at https://doi.org/10.1016/j.eurpolymj.2021.110536.

References

[1] C. Delloye, O. Cornu, V. Druez, O. Barbier, Bone allografts: What they can offer and what they cannot, J. Bone Joint Surg. Br. 89 (5) (2007), 574 9.
[2] H. Petite, V. Viateau, W. Bensaïd, A. Meunier, C. de Pollak, M. Bourguignon, K. Oudina, L. Sedel, G. Guillemin, Tissue-engineered bone regeneration, Nat. Biotechnol. 18 (9) (2000) 959–963.
[3] S.K. Nandi, S. Roy, P. Mukherjee, B. Kundu, D.K. De, D. Basu, Orthopaedic applications of bone graft & graft substitutes: a review, Indian J. Med. Res. 132 (2010) 15–30.
[4] M.E. Elsalanty, D.G. Genecov, Bone grafts in craniofacial surgery, Craniomaxillofac. Trauma Reconstr. 2 (3) (2009) 125–134.
[5] V.T. Athanasiou, D.J. Papachristou, A. Panagopoulos, A. Saridis, C.D. Scopa, P. Megas, Histological comparison of autograft, allograft-DBM, xenograft, and synthetic grafts in a trabecular bone defect: an experimental study in rabbits, Med. Sci. Monit. 16 (1) (2010).
[6] G. Zimmermann, A. Moghaddam, Allograft bone matrix versus synthetic bone graft substitutes, Injury 42 (Suppl 2) (2011) S16–S21.

[7] P. Janicki, G. Schmidmaier, What should be the characteristics of the ideal bone graft substitute? Combining scaffolds with growth factors and/or stem cells, Injury 42 (2011) S77–S81.
[8] D.M. Ehrler, A.R. Vaccaro, The use of allograft bone in lumbar spine surgery, Clin. Orthop. Relat. Res. 371 (2000) 38–45.
[9] C. Delloye, Tissue allografts and health risks, Acta Orthop. Belg. 60 (Suppl 1) (1994) 62–67.
[10] J.E. Fleming, C.N. Cornell, G.F. Muschler, Bone cells and matrices in orthopedic tissue engineering, Orthop. Clin. North Am. 31 (3) (2000) 357–374.
[11] C.R. Perry, Bone repair techniques, bone graft, and bone graft substitutes, Clin. Orthop. Relat. Res. 360 (1999) 71–86.
[12] A. Oryan, A. Moshiri, S. Alidadi, Current concerns regarding healing of bone defects, Hard Tissue 2 (2013) 13.
[13] K. Gomes, J. Carlini, C. Biron, A. Rapoport, R. Dedivitis, Use of Allogeneic Bone Graft in Maxillary Reconstruction for Installation of Dental Implants, J. Oral Maxillofacial Surg. Off J. Am. Ass. Oral Max Surg. 66 (2008) 2335–2338.
[14] R. Detsch, A.R. Boccaccini, The role of osteoclasts in bone tissue engineering, J. Tissue Eng. Regen. Med. 9 (10) (2015) 1133–1149.
[15] J.P. Sapp, An ultrastructural study of nuclear and centriolar configurations in multinucleated giant cells, Lab. Invest. 34 (2) (1976) 109–114.
[16] R. Baron, L. Neff, D. Louvard, P.J. Courtoy, Cell-mediated extracellular acidification and bone resorption: evidence for a low pH in resorbing lacunae and localization of a 100-kD lysosomal membrane protein at the osteoclast ruffled border, J. Cell Biol. 101 (6) (1985) 2210–2222.
[17] T.J. Chambers, The birth of the osteoclast, Ann. N. Y. Acad. Sci. 1192 (2010) 19–26.
[18] T.J. Martin, N.A. Sims, Osteoclast-derived activity in the coupling of bone formation to resorption, Trends Mol. Med. 11 (2) (2005) 76–81.
[19] H.K. Vaananen, H. Zhao, M. Mulari, J.M. Halleen, The cell biology of osteoclast function, J. Cell Sci. 113 (3) (2000) 377–381.
[20] T.M. Gregory, E.C. Moreno, J.M. Patel, W.E. Brown, Solubility of β-Ca(3)(PO(4))(2) in the System Ca(OH)(2)-H(3)PO(4)-H(2)O at 5, 15, 25, and 37 °C, J. Res. Natl. Bur. Stand A Phys. Chem. 78A (6) (1974) 667–674.
[21] H. Blair, S. Teitelbaum, R. Ghiselli, S. Gluck, Osteoclastic bone resorption by a polarized vacuolar proton pump, Science 245 (4920) (1989) 855–857.
[22] I.A. Silver, R.J. Murrills, D.J. Etherington, Microelectrode studies on the acid microenvironment beneath adherent macrophages and osteoclasts, Exp. Cell Res. 175 (2) (1988) 266–276.
[23] S.-H. Lee, H. Shin, Matrices and scaffolds for delivery of bioactive molecules in bone and cartilage tissue engineering, Adv. Drug Del. Rev. 59 (4) (2007) 339–359.
[24] S.M. Schnürer, U. Gopp, K.D. Kühn, S.J. Breusch, Knochenersatzwerkstoffe, Der Orthopäde 32 (1) (2003) 2–10.
[25] Y.-C. Chen, R.-Z. Lin, H. Qi, Y. Yang, H. Bae, J.M. Melero-Martin, A. Khademhosseini, Functional Human Vascular Network Generated in Photocrosslinkable Gelatin Methacrylate Hydrogels, Adv. Funct. Mater. 22 (10) (2012) 2027–2039.
[26] M. Schuster, C. Turecek, G. Weigel, R. Saf, J. Stampfl, F. Varga, R. Liska, Gelatin-based photopolymers for bone replacement materials, J. Polym. Sci., Part A: Polym. Chem. 47 (24) (2009) 7078–7089.
[27] A. Ovsianikov, A. Deiwick, S. Van Vlierberghe, M. Pflaum, M. Wilhelmi, P. Dubruel, B. Chichkov, Laser Fabrication of 3D Gelatin Scaffolds for the Generation of Bioartificial Tissues, Materials 4 (1) (2011).
[28] D.A. Wahl, J.T. Czernuszka, Collagen-hydroxyapatite composites for hard tissue repair, Eur. Cells Mater. 11 (2006) 43–56.
[29] K.P. Sai, M. Babu, Collagen based dressings — a review, Burns 26 (1) (2000) 54–62.
[30] A.J. Salgado, O.P. Coutinho, R.L. Reis, Bone Tissue Engineering: State of the Art and Future Trends, Macromol. Biosci. 4 (8) (2004) 743–765.
[31] D.S. Katti, S. Lakshmi, R. Langer, C.T. Laurencin, Toxicity, biodegradation and elimination of polyanhydrides, Adv. Drug Del. Rev. 54 (7) (2002) 933–961.
[32] V. Tangpasuthadol, S.M. Pendharkar, J. Kohn, Hydrolytic degradation of tyrosine-derived polycarbonates, a class of new biomaterials. Part I: Study of model compounds, Biomaterials 21 (23) (2000) 2371–2378.
[33] C. Heller, M. Schwentenwein, G. Russmüller, T. Koch, D. Moser, C. Schopper, F. Varga, J. Stampfl, R. Liska, Vinylcarbonates and vinylcarbamates: Biocompatible monomers for radical photopolymerization, J. Polym. Sci., Part A: Polym. Chem. 49 (3) (2011) 650–661.
[34] H.W. Vohr, Toxikologie: Band 2 - Toxikologie der Stoffe, Wiley, 2012.
[35] A. Moreno, G. Lligadas, J.C. Ronda, M. Galià, V. Cádiz, Linear and branched acetal polymers from castor oil via acetal metathesis polymerization, Eur. Polym. J. 108 (2018) 348–356.
[36] P.H. Warnke, H. Seitz, F. Warnke, S.T. Becker, S. Sivananthan, E. Sherry, Q. Liu, J. Wiltfang, T. Douglas, Ceramic scaffolds produced by computer-assisted 3D printing and sintering: Characterization and biocompatibility investigations, J. Biomed. Mater. Res. Part B: Appl. Biomater. 93B (1) (2010) 212–217.
[37] E.E. Falco, M. Patel, J.P. Fisher, Recent Developments in Cyclic Acetal Biomaterials for Tissue Engineering Applications, Pharm. Res. 25 (10) (2008) 2348–2356.
[38] M.W. Betz, J.F. Caccamese, D.P. Coletti, J.J. Sauk, J.P. Fisher, Tissue response and orbital floor regeneration using cyclic acetal hydrogels, J. Biomed. Mater. Res. Part A 90A (3) (2009) 819–829.
[39] M.W. Betz, P.C. Modi, J.F. Caccamese, D.P. Coletti, J.J. Sauk, J.P. Fisher, Cyclic acetal hydrogel system for bone marrow stromal cell encapsulation and osteodifferentiation, J. Biomed. Mater. Res. Part A 86A (3) (2008) 662–670.
[40] M.W. Betz, A.B. Yeatts, W.J. Richbourg, J.F. Caccamese, D.P. Coletti, E.E. Falco, J. P. Fisher, Macroporous Hydrogels Upregulate Osteogenic Signal Expression and Promote Bone Regeneration, Biomacromolecules 11 (5) (2010) 1160–1168.
[41] B.M. Alameda, T.C. Palmer, J.D. Sisemore, N.G. Pierini, D.L. Patton, Hydrolytically degradable poly(β-thioether ester ketal) thermosets via radical-mediated thiol–ene photopolymerization, Polym. Chem. 10 (41) (2019) 5635–5644.
[42] D.G. Sycks, D.L. Safranski, N.B. Reddy, E. Sun, K. Gall, Tough Semicrystalline Thiol-Ene Photopolymers Incorporating Spiroacetal Alkenes, Macromolecules 50 (11) (2017) 4281–4291.
[43] D.G. Sycks, T. Wu, H.S. Park, K. Gall, Tough, stable spiroacetal thiol-ene resin for 3D printing, J. Appl. Polym. Sci. 135 (22) (2018) 46259.
[44] S. Lingier, P. Espeel, S.S. Suarez, O. Türünç, S. De Wildeman, F.E. Du Prez, Renewable thermoplastic polyurethanes containing rigid spiroacetal moieties, Eur. Polym. J. 70 (2015) 232–239.
[45] C. Gorsche, R. Harikrishna, S. Baudis, P. Knaack, B. Husar, J. Laeuger, H. Hoffmann, R. Liska, Real Time-NIR/MIR-Photorheology: A Versatile Tool for the in Situ Characterization of Photopolymerization Reactions, Anal. Chem. 89 (9) (2017) 4958–4968.
[46] P. Deslongchamps, Y.L. Dory, S. Li, The Relative Rate of Hydrolysis of a Series of Acyclic and Six-Membered Cyclic Acetals, Ketals, Orthoesters, and Orthocarbonates, Tetrahedron 56 (22) (2000) 3533–3537.
[47] P.G.M. Wuts (Eds.), Greene's Protective Groups in Organic Synthesis, fifth ed., Wiley, 2014, pp. 1400.
[48] B. Liu, S. Thayumanavan, Substituent Effects on the pH Sensitivity of Acetals and Ketals and Their Correlation with Encapsulation Stability in Polymeric Nanogels, J. Am. Chem. Soc. 139 (6) (2017) 2306–2317.
[49] A. Hufendiek, S. Lingier, F.E. Du Prez, Thermoplastic polyacetals: chemistry from the past for a sustainable future? Polym. Chem. (2018).
[50] T.H. Fife, L.K. Jao, Substituent Effects in Acetal Hydrolysis, J. Org. Chem. 30 (5) (1965) 1492–1495.
[51] A.S.Y. Lee, C.L. Cheng, A novel and selective method for hydrolysis of acetals and ketals, Tetrahedron 53 (42) (1997) 14255–14262.
[52] N. Moszner, T. Hirt, New polymer-chemical developments in clinical dental polymer materials: Enamel–dentin adhesives and restorative composites, J. Polym. Sci., Part A: Polym. Chem. 50 (21) (2012) 4369–4402.
[53] S. Tielens, H. Declercq, T. Gorski, E. Lippens, E. Schacht, M. Cornelissen, Gelatin-Based Microcarriers as Embryonic Stem Cell Delivery System in Bone Tissue Engineering: An in-Vitro Study, Biomacromolecules 8 (3) (2007) 825–832.
[54] A. Tiwari, J.J. Grailer, S. Pilla, D.A. Steeber, S. Gong, Biodegradable hydrogels based on novel photopolymerizable guar gum-methacrylate macromonomers for in situ fabrication of tissue engineering scaffolds, Acta Biomater. 5 (9) (2009) 3441–3452.
[55] S.F. Marrian, The Chemical Reactions of Pentaerythritol and its Derivatives, Chem. Rev. 43 (1) (1948) 149–202.
[56] O. Wichterle, D. Lím, Hydrophilic Gels for Biological Use, Nature 185 (1960) 117.
[57] P.H. Corkhill, C.J. Hamilton, B.J. Tighe, Synthetic hydrogels VI. Hydrogel composites as wound dressings and implant materials, Biomaterials 10 (1) (1989) 3–10.
[58] P.A. Netti, J.C. Shelton, P.A. Revell, G. Pirie, S. Smith, L. Ambrosio, L. Nicolais, W. Bonfield, Hydrogels as an interface between bone and an implant, Biomaterials 14 (14) (1993) 1098–1104.
[59] J. Biscarat, B. Galea, J. Sanchez, C. Pochat-Bohatier, Effect of chemical cross-linking on gelatin membrane solubility with a non-toxic and non-volatile agent: Terephthalaldehyde, Int. J. Biol. Macromol. 74 (2015) 5–11.
[60] L.P.D. Ratcliffe, A.J. Ryan, S.P. Armes, From a Water-Immiscible Monomer to Block Copolymer Nano-Objects via a One-Pot RAFT Aqueous Dispersion Polymerization Formulation, Macromolecules 46 (3) (2013) 769–777.
[61] C. Gorsche, K. Seidler, P. Knaack, P. Dorfinger, T. Koch, J. Stampfl, N. Moszner, R. Liska, Rapid formation of regulated methacrylate networks yielding tough materials for lithography-based 3D printing, Polym. Chem. 7 (11) (2016) 2009–2014.
[62] N. Moszner, U.K. Fischer, B. Ganster, R. Liska, V. Rheinberger, Benzoyl germanium derivatives as novel visible light photoinitiators for dental materials, Dent. Mater. 24 (7) (2008) 901–907.
[63] S.C. Ligon, R. Liska, J. Stampfl, M. Gurr, R. Mülhaupt, Polymers for 3D Printing and Customized Additive Manufacturing, Chem. Rev. 117 (15) (2017) 10212–10290.
[64] T. Mezger, Applied Rheology: With Joe Flow on Rheology Road, Paar (2015).
[65] P. Frasca, R. Harper, J.L. Katz, Strain and frequency dependence of shear storage modulus for human single osteons and cortical bone microsamples—Size and hydration effects, J. Biomech. 14 (10) (1981) 679–690.
[66] J. Henkel, M.A. Woodruff, D.R. Epari, R. Steck, V. Glatt, I.C. Dickinson, P.F. M. Choong, M.A. Schuetz, D.W. Hutmacher, Bone Regeneration Based on Tissue Engineering Conceptions - A 21st Century Perspective, Bone research 1 (3) (2013) 216–248.
[67] S. Nair L, T. Laurencin C, Biodegradable Polymers as, Biomaterials. 32 (2007) 762–798.
[68] S. Li, Hydrolytic degradation characteristics of aliphatic polyesters derived from lactic and glycolic acids, J. Biomed. Mater. Res. 48 (3) (1999) 342–353.
[69] K.J. Zhu, R.W. Hendren, K. Jensen, C.G. Pitt, Synthesis, properties, and biodegradation of poly(1,3-trimethylene carbonate), Macromolecules 24 (8) (1991) 1736–1740.
[70] Y. Zhou, Y. Dan, L. Jiang, G. Li, The effect of crystallization on hydrolytic stability of polycarbonate, Polym. Degrad. Stab. 98 (8) (2013) 1465–1472.
[71] R.F. Atkinson, T.C. Bruice, Ring strain and general acid catalysis of acetal hydrolysis. Lysozyme catalysis, *J. Am. Chem. Soc.* 96 (3) (1974) 819–825.

[72] J.P. Knowles, A. Whiting, The Effects of Ring Size and Substituents on the Rates of Acid-Catalysed Hydrolysis of Five- and Six-Membered Ring Cyclic Ketone Acetals, Eur. J. Org. Chem. 2007 (20) (2007) 3365–3368.
[73] J.A. Tamada, R. Langer, Erosion kinetics of hydrolytically degradable polymers, Proc. Natl. Acad. Sci. U. S. A. 90 (2) (1993) 552–556.
[74] A. Göpferich, Mechanisms of polymer degradation and erosion, Biomaterials 17 (2) (1996) 103–114.